Evaluation of enamel crystallites in subsurface lesion by microbeam X-ray diffraction

N. Yagi,[a]* N. Ohta,[a] T. Matsuo,[a] T. Tanaka,[b] Y. Terada,[b] H. Kamasaka,[b] K. To-o,[b] T. Kometani[b] and T. Kuriki[c]

[a]Japan Synchrotron Radiation Research Institute, 1-1-1 Kouto, Sayo, Hyogo 679-5198, Japan, [b]Health Science Laboratory, Ezaki Glico Co. Ltd, 4-6-5 Utajima, Nishiyodogawa-ku, Osaka 555-8502, Japan, and [c]Biochemical Research Laboratory, Ezaki Glico Co. Ltd, 4-6-5 Utajima, Nishiyodogawa-ku, Osaka 555-8502, Japan. E-mail: yagi@spring8.or.jp

Early caries lesion is a demineralization process that takes place in the top 0.1 mm layer of tooth enamel. In this study, X-ray microbeam diffraction was used to evaluate the hydroxyapatite crystallites in the subsurface lesion of a bovine enamel section and the results are compared with those obtained by transversal microradiography, a method commonly used for evaluation of tooth mineral. Synchrotron radiation from SPring-8 was used to obtain a microbeam with a diameter of 6 μm. Wide-angle X-ray diffraction reports the amount of hydroxyapatite crystals, and small-angle X-ray scattering reports that of voids in crystallites. All three methods showed a marked decrease in the enamel density in the subsurface region after demineralization. As these diffraction methods provide structural information in the nanometre range, they are useful for investigating the mechanism of the mineral loss in early caries lesion at a nanometre level.

Keywords: X-ray diffraction; transversal microradiography; enamel; lesion.

1. Introduction

An early caries lesion in tooth enamel is caused by acids produced by bacteria in dental plaque and dentally observed as a white opaque spot. In a cross section along the direction perpendicular to the enamel surface, a caries lesion appears as an enamel decay with a relatively intact surface layer and a mineral loss in the subsurface region (Arends & Christoffersen, 1986). When not treated, the decay spreads to the dentin and forms a cavity. Over the past three decades, many studies have been made to evaluate demineralization of the early subsurface lesion under different conditions. Most of these studies used transversal microradiography (TMR) (Damen *et al.*, 1977) to measure the mineral contents. The TMR analysis measures the mineral uptake or loss directly from microradiography of thin sections of enamel and is regarded as a primary standard method for demineralization analyses (Featherstone & Zero, 1992; ten Cate *et al.*, 1996). However, since evidence on the crystal structure of hydroxyapatite (HAp), which comprises tooth enamel, cannot be obtained by this method, the apparent change in mineral content may be partially due to change in other substances. The enamel HAp is arranged in rod-like units called crystallites. The morphology of HAp crystallites was studied by high-resolution transmission electron microscopy and the decrease in the HAp crystal size by demineralization was reported (Featherstone, 1979). However, correspondence between the

TMR results and microscopy has not been reported, mainly because electron microscopy suffers from sample damage during preparation. Thus, in order to quantitatively compare the TMR results with the fine structure of the HAp crystallites, a different technique is needed.

In the present study, we used a microbeam X-ray diffraction technique to investigate the HAp crystallites in the subsurface lesion. X-ray diffraction provides structural information on the HAp crystallites at submicrometre and atomic levels. Namely, the wide-angle X-ray diffraction (WAXRD) arises from the crystals of HAp and thus its intensity generally correlates with the amount of crystals, while the small-angle X-ray diffraction (SAXS) provides evidence of the arrangement of larger objects in the sample, which are crystallites in the case of enamel. The microbeam (6 μm diameter) was small enough to study the 100 μm-thick subsurface lesion and enabled us to compare the crystallite structure with the TMR results at the spatial resolution required for the analysis of the lesion.

2. Materials and methods

2.1. Preparation of artificial subsurface lesion

Bovine incisors were obtained from a local slaughterhouse (Osaka, Japan). Enamel blocks (∼7 mm × 7 mm × 3 mm depth) were cut out and embedded in resin (GC CORP,

Japan). The blocks were polished on a wet polishing paper (3M wrapping paper 800, 1000 and 2000 grid, USA) to expose a sound and flat enamel surface. Then, sound and demineralized zones were made on the same enamel surface as follows. First, half of each block surface was covered with a nail varnish as described (Meyer-Lueckel *et al.*, 2006). Then, subsurface lesions were formed by demineralization in a two-layer system of 8% methyl cellulose gel (Fluka, USA) and 0.1 M lactate buffer (pH 4.6) at 310 K for 14 days (ten Cate *et al.*, 1996). After lesions were made in the demineralized zone by acid treatment, the nail varnish was washed with acetone to reveal the intact sound zone.

2.2. TMR

After the demineralization treatment, the enamel blocks were cut from the middle of each block into sections of approximately 150 µm thickness perpendicularly to the surface, using a water-cooled diamond-coated wire saw (Well Diamond Wire Saws, Germany). The thin sections were microradiographed onto high-resolution plates (Konica Minolta Opto, Japan) with Cu $K\alpha$ X-rays generated at 20 kV and 20 mA for 13 min (PW-3830, Philips, Netherlands). The mineral profiles of the sound and demineralized zones were obtained from the digital images of the microradiographs.

2.3. WAXRD and SAXS measurements with an X-ray microbeam

The experiments were carried out at the BL40XU beamline (Fig. 1) (Inoue *et al.*, 2001) of the SPring-8 third-generation synchrotron radiation facility with an X-ray energy of 15.0 keV (bandwidth ~3%). An X-ray microbeam was obtained by placing a pinhole in the focused beam (Ohta *et al.*, 2005). The diameter of the beam at the sample was about 6 µm (full width at half-maximum). The X-ray flux was about 3×10^{11} photons s^{-1}. The sample-to-detector distance was 180 mm for WAXRD (Fig. 1b) and about 3000 mm for SAXS (Fig. 1a). The reciprocal spacing was calibrated with a powder diffraction pattern of LaB$_6$ for WAXRD and the meridional reflections from dried chicken tendon collagen (first order at 63 nm) for SAXS. The reciprocal spacing is expressed as $q = 4\pi \sin\theta/\lambda$, where 2θ is the scattering angle and λ is the wavelength of the X-ray. The X-ray detector consisted of an X-ray image intensifier (V5445P, Hamamatsu Photonics, Hamamatsu, Japan) (Amemiya *et al.*, 1995) coupled to a cooled CCD camera (ORAC-II-ER, Hamamatsu Photonics). In some experiments the SAXS and WAXRD patterns were recorded simultaneously with a flat-panel detector (C9728DK, Hamamatsu Photonics) (Yagi & Inoue, 2007) for WAXRD (Fig. 1c). An ionization chamber (S-1329, Oken, Tokyo) was also inserted between the flat-panel detector and the vacuum tube to measure the transmission of the X-rays through the sample.

The enamel sections, which had been examined by TMR, were subjected to the SAXS measurements (Fig. 1a). The sections had been kept sealed with water, but all X-ray measurements were made at ambient temperature and humidity. A section was mounted vertically so that its enamel
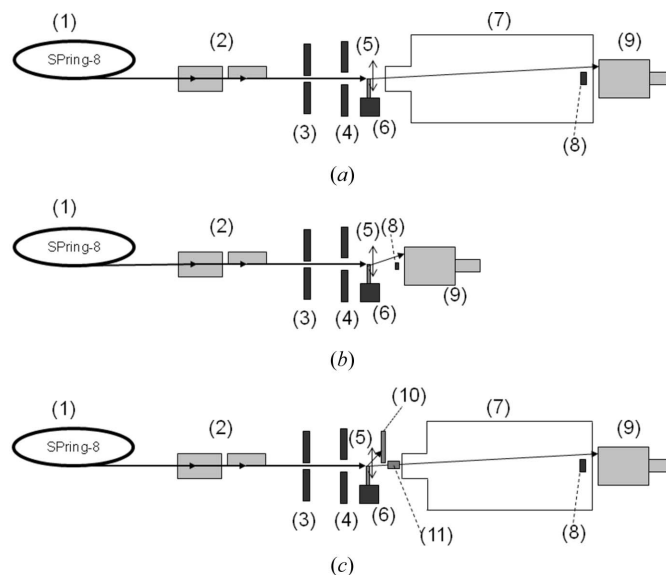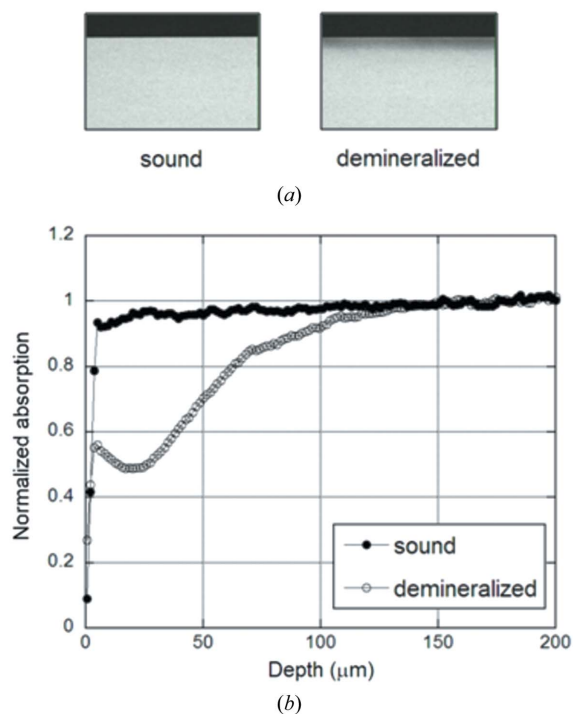

Figure 1
Schematic diagrams of the X-ray measurement set-up at BL40XU in the SPring-8 synchrotron radiation facility. (a) Arrangement for the small-angle X-ray diffraction (SAXS) measurement, (b) arrangement for the wide-angle X-ray scattering (WAXRD) measurement, (c) arrangement for the simultaneous SAXS/WAXRD measurement. The numbers indicate the following items: (1) synchrotron X-ray source (SPring-8), (2) two focusing mirrors, (3) collimating pinhole (about 5 µm diameter), (4) guard pinhole (25–50 µm diameter), (5) specimen (thin slice of bovine enamel), (6) remote-controlled vertical translation stage, (7) vacuum pipe to eliminate air scatter, (8) beam stop to avoid exposure of the direct beam on the detector, (9) X-ray detector (an image intensifier combined with a cooled CCD camera), (10) flat-panel X-ray detector, (11) ionization chamber. Approximate distances are: from (1) to (2) 40 m, (2) to (3) 10 m, (3) to (4) 50 mm, (4) to (5) 10 mm, (5) to (8) 3 m in (a). The distance from (5) to (8) in (b) was about 100 mm.

edge was horizontal. The X-ray beam passed perpendicularly through the slice. The sample was moved upwards with 5 µm steps so that the X-ray beam scanned across the enamel from the surface towards the dentin. At each step a SAXS pattern was recorded. A region to a depth of 200 µm was scanned. The sound and demineralized zones of each sample were studied. Then, the same samples were subjected to the WAXRD measurement with a shorter sample-to-detector distance using the same procedure (Fig. 1b).

3. Results

3.1. TMR

TMR is a laboratory technique commonly used to evaluate the mineral loss in tooth enamel. It uses an X-ray microradiograph to measure absorption of X-rays and converts it to mineral density. Fig. 2 shows the absorption profiles of the sound and demineralized zones in bovine enamel sections obtained by densitometry of the high-resolution plate. The profiles are obtained from the surface to the inner region of the enamel. In the sound zone, the absorption is almost flat showing that the mineral density is constant in the enamel. The small increase in absorption in the deeper region may be due to an increase in thickness of the sample. Note that the
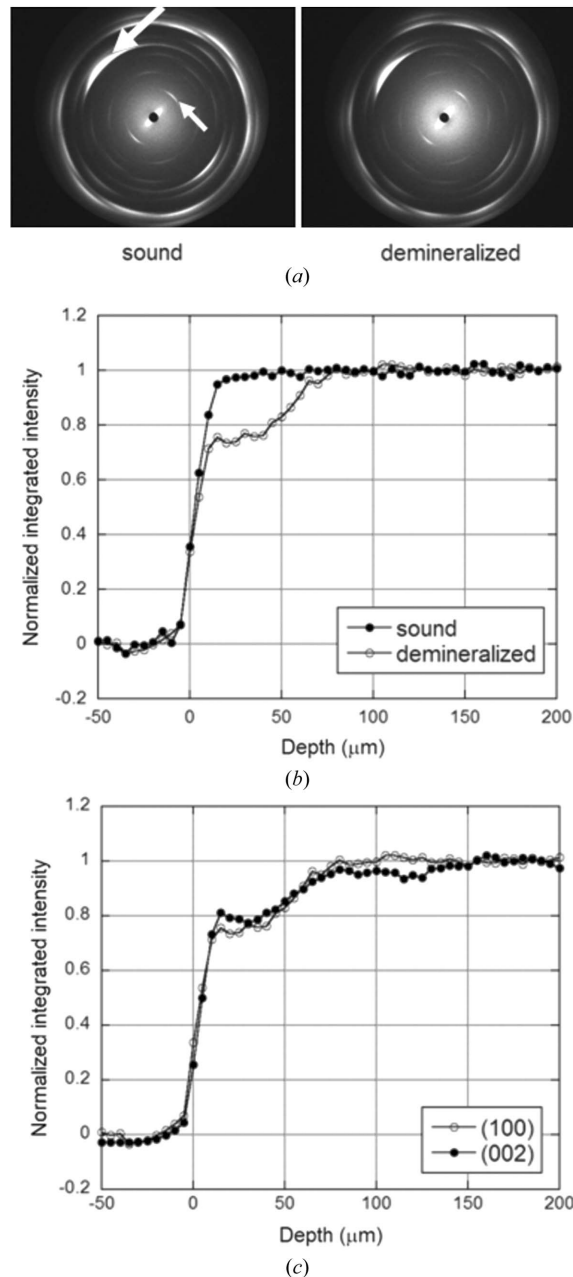
sound   demineralized

(a)

(b)

Figure 2
Early caries lesions studied with transmission microradiography. (a) Microradiographs of the sound and demineralized zones with the enamel surface at the top. The dark zone at the top is where there is no sample. The sound enamel is almost uniform in density, while in the demineralized zone the region close to the surface is dark, showing less absorption of X-rays. This corresponds to the subsurface lesion. (b) Typical mineral distributions in bovine enamel obtained by microradiography after demineralization (open circles) in comparison with the untreated sound enamel (filled circles).

surface of the enamel is not that of the tooth because it was exposed by polishing. On the other hand, in the demineralized zone there is a region within 100 μm from the surface where the absorption is small, which is the region of the subsurface lesion. This result demonstrates a decrease in density owing to the acid treatment.

In the demineralized zone the surface layer to a depth of about 20 μm has a higher density than the deeper region (Fig. 2). This relatively unaffected layer is characteristic of the method of demineralization employed here (ten Cate *et al.*, 1996) and commonly observed in human carious lesion in its early stage (Silverstone, 1977).

3.2. WAXRD

The WAXRD pattern from a slice of bovine enamel shows diffraction from the HAp crystallites (Fig. 3a). The HAp microcrystals (crystallites) in the enamel are 0.05–0.2 μm in diameter and up to a few micrometres in length (Arends & Jongebloed, 1978; Kerebel *et al.*, 1979). The long axis corresponds to the *c*-axis of the unit cell of the HAp crystal. The crystallites are arranged with their *c*-axes almost parallel to each other but their rotation around the *c*-axis is random. Thus, the WAXRD pattern from the enamel resembles that of fibrous materials and the diffraction spots can be indexed on a

sound   demineralized

(a)

(b)

(c)

Figure 3
Wide-angle X-ray diffraction patterns from bovine enamel in the sound and demineralized zones recorded with an X-ray image intensifier and a CCD camera. (a) Diffraction patterns from the sound and demineralized zones at about 30 μm from the surface. The exposure time was 300 ms. The small arrow in the sound pattern indicates the (100) equatorial reflections from the HAp crystallites. The large arrow indicates the (002) meridional reflection. The direction of the *c*-axis of the HAp crystal is parallel to the meridian. The isotropic scattering around the backstop is higher in the demineralized pattern, which is likely to be due to the increase in the void volume by demineralization as shown by the SAXS results (Fig. 4). (b) Changes in the integrated (100) intensity with the depth in the enamel. Scans in six different areas were made in the sound and demineralized zones of each enamel sample, and the results were averaged in each zone. Then, to compensate for the difference in the thickness of the sample, the result from each area was normalized by the average intensity in the 150–200 μm region. The plot is an average of data from five samples from different teeth. (c) Comparison of the intensity changes of the equatorial (100) and the meridional (002) reflections. The meridional reflection has more fluctuation in intensity because of the tilt of the *c*-axis towards the X-ray beam affects its intensity.

hexagonal three-dimensional lattice (Trautz *et al.*, 1953). The diffraction spots are arced because the crystallites are not pointing in the same direction throughout the path of the X-ray beam in the sample. However, the widths across the arcs in the radial direction are similar to the X-ray energy spread (about 3%), suggesting that the perfection in each crystallite is high. In most samples the *c*-axis of the crystallite (that is, the meridian) was inclined by about 45° from the surface of the enamel that was more or less parallel to the surface of the tooth. Although not pronounced in Fig. 3(*a*), two sets of diffraction diagrams with different orientations were often superimposed, with the *c*-axes tilted by about 90° from each other ('two fibre axes' patterns) (Hirota, 1986).

The two symmetrical (002) meridional spots, one of which is indicated by the larger arrow in the pattern from the sound zone in Fig. 3(*a*), are quite different in intensity, but the (100) equatorial spots, one of which is indicated by the smaller arrow, are similar in intensity. This is because the intensity of the meridional reflections was affected by a tilt of the *c*-axis towards the X-ray beam: in extreme cases, when the *c*-axis is excessively tilted, the meridional reflections do not cross the Ewald sphere in the reciprocal space and are not observed in the diffraction pattern. Since the tilt of the needle-shaped HAp crystallites varies from area to area, this leads to a variation in the intensity measured along the depth in the enamel (Fig. 3*c*). On the other hand, since the rotation of the crystallites around their *c*-axes is random, the equatorial reflections are continuous rings in the reciprocal space and always cross the Ewald sphere. They are always observed regardless of the orientation of the crystallites, making their intensity more reliable as an index of the amount of the HAp crystallites. Although a correction has to be made when the tilt of the *c*-axis varies greatly, the range of the tilt was not large in our enamel samples, as can be judged by the fluctuation of the (002) intensity (Fig. 3*c*). Thus, the two-dimensionally integrated intensity of the (100) equatorial reflection (at a Bragg spacing of 0.815 nm) after background subtraction was measured as an index of the amount of the HAp crystallites.

When the integrated intensity of the (100) peak was plotted against the distance of the X-ray beam from the surface, it was almost constant in the sound zone but lower within about 100 µm below the surface in the demineralized zone (Fig. 3*b*). This result is similar to that for TMR (Fig. 2*b*). The radial widths (full width at half-maximum) of the (100) and (002) peaks were 0.06 and 0.21 nm^{-1}, respectively, in the control enamel. Within the resolution of the present study (the width is determined mostly by the energy bandwidth as explained above), these values did not change significantly along the depth or by demineralization (data not shown).

3.3. SAXS

The SAXS patterns from the sound enamel showed a weak equatorial scatter, that is, at right angles to the *c*-axis of the HAp crystallites (Fig. 4*a*). In analogy to fibre diffraction patterns (Fraser & MacRae, 1974), the scatter is likely to be due to the density difference between the needle-shaped HAp crystallites and the matrix between them which is composed of lighter non-mineral substances including water and carbonate.

In the demineralized zone, the equatorial scatter was greatly enhanced in the region about 100 µm from the surface (Fig. 4*b*). Increase in the scatter in the small angles is also evident in the WAXRD pattern (Fig. 3*a*). This region corresponds to that of mineral loss found by TMR and WAXRD. Since it has been known that decalcification by acid treatment creates longitudinal voids in the matrix regions by reducing the size of the HAp crystallites (Simmelink & Abrigo, 1989), the SAXS enhancement is interpreted to be due to formation of voids in the enamel. This scatter from voids is similar to the SAXS from carbon fibre (Gupta *et al.*, 1994) and cellulose (Crawshaw & Cameron, 2000). The SAXS from a powdered enamel sample was interpreted in the same manner (Gutierrez *et al.*, 2005), but, to the authors' knowledge, the present study is the first to demonstrate that the voids are concentrated in the subsurface area. The equatorial scatter (Fig. 4*c*) is rather featureless and difficult to interpret. Since the voids cannot be assumed to be spherical, it is difficult to use standard software for the analysis. However, the scattering profile from the demineralized zone is steeper in the small-angle region ($q < 0.2$ nm^{-1}) than that from the sound zone, suggesting that there is a population of larger voids in the demineralized zone. Fig. 4(*d*) shows the depth dependence of the SAXS profile in the demineralized zone. Although not as conspicuous as in Fig. 4(*c*), the curves cannot be superimposed by simple translation. The scattering at the small angles is higher in the demineralized region (depth 40 µm) than in the unaffected region (200 µm). This tendency is also seen at the region (120 µm) where the WAXRD was not affected, and especially pronounced near the surface (10 µm). These results suggest that not only the number but the size and shape of the voids vary with depth.

In some experiments the SAXS and the WAXRD were measured simultaneously (Fig. 1*c*). In this case the WAXRD was measured with a CMOS flat-panel detector (Yagi & Inoue, 2007) which could record only less than a half of the diffraction pattern (Fig. 5*a*). However, since the direction of the equator was usually confined to the azimuth of about 45° from the surface, by adjusting the orientation of the detector it was possible to monitor the intensity of one (100) diffraction spot (Fig. 5*b*). A simultaneous measurement of X-ray transmission through the sample with an ionization chamber (Fig. 5*c*) is equivalent to TMR. The SAXS data were obtained at about 3 m downstream with an X-ray image intensifier and a CCD camera (Fig. 5*d*). This simultaneous measurement ensures that the transmission, SAXS and WAXRD data are obtained at the same spot of the same sample, facilitating comparison of these data.

As exactly the same part of the sample was interrogated by the three techniques, two interesting features can be pointed out. One is the surface layer with higher density that is clearly seen with TMR (Fig. 2). This is less distinct in the absorption (Fig. 5*c*) because of the lack of spatial resolution that is apparent in the gradual rise of absorption at the edge. Although the full width at half-maximum of the microbeam is

(a)

(b)

(c)

(d)
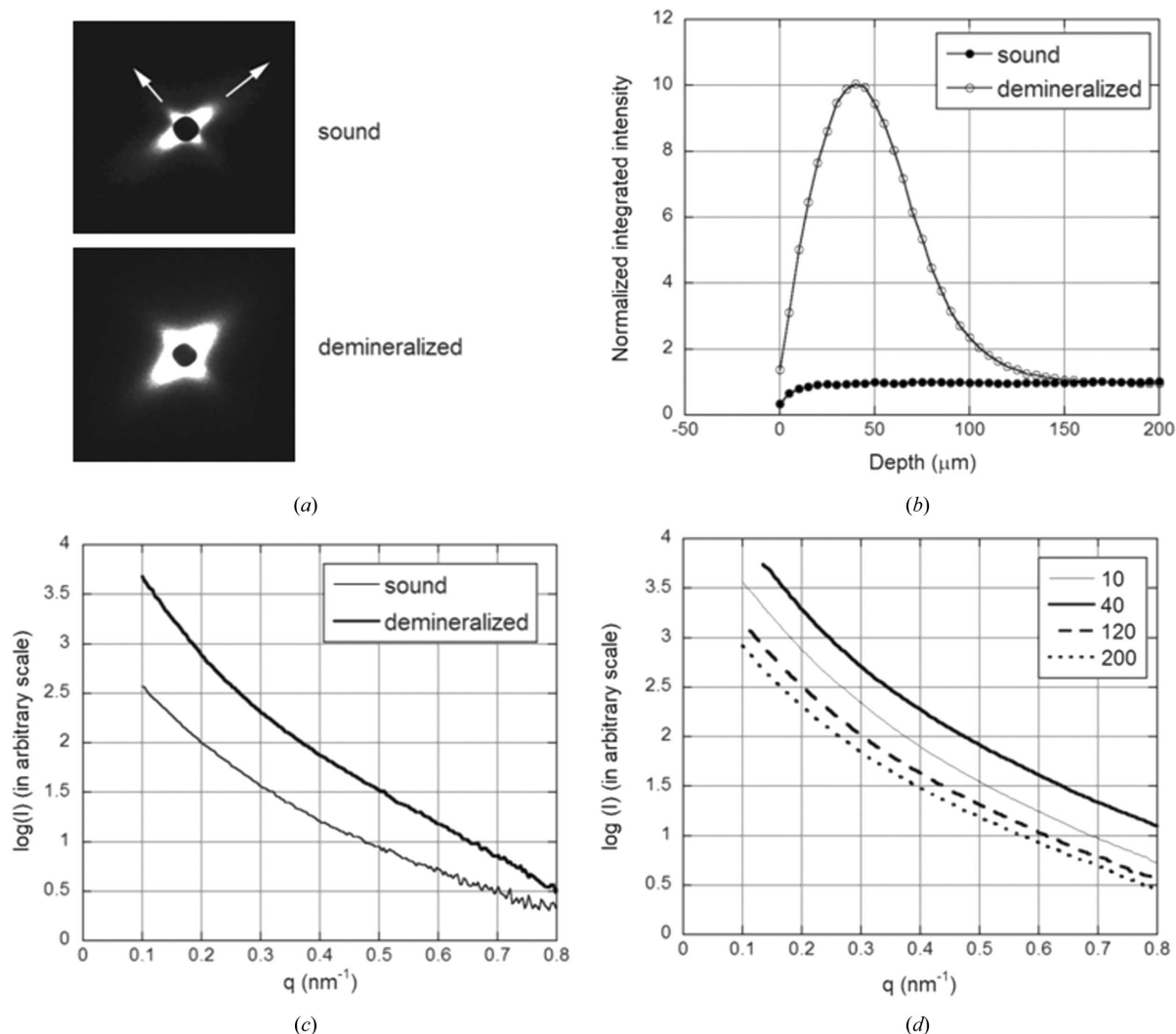
Figure 4
Small-angle X-ray scattering patterns from bovine enamel recorded with an X-ray image intensifier and a CCD camera. (a) Patterns from the sound and demineralized zones at a depth of about 35 μm from the surface. The exposure time was 100 ms. These patterns show the superposition of two sets of diffraction diagrams with different orientations (Hirota, 1986). Approximate directions of the two equators, which are at right angles to the c-axes, are shown by arrows in the pattern from the sound zone. (b) Changes in the total equatorial scattering intensity with the depth in the enamel. Since only the equatorial scatter was observed, the total scattering intensity was obtained by summing the intensity in all directions in the region $q > 0.094$ nm^{-1}. Three scans in different areas were made in the sound and demineralized zones of each enamel sample, and the results were averaged in each area. Then, to compensate for the difference in the thickness of the sample, the result from each area was normalized by the average intensity in the 150–200 μm region. The plot is an average of data from five samples of different teeth. (c) Equatorial intensity profiles at a depth of about 35 μm from the surface in sound and demineralized enamels. (d) Equatorial intensity profiles at four different depths (10, 40, 120, 200 μm) from the surface in demineralized enamel.

about 6 μm, there is a considerably long tail owing to Fresnel fringes from the pinhole. Also, the enamel sample may not be set up with its surface edge exactly parallel to the X-ray beam. Compared with the absorption, the 20 μm layer has even lower intensity in the WAXRD data (Fig. 5b). This may show that the surface layer contains a lower amount of HAp crystallites per density, but a study at higher spatial resolution will be required to confirm this.

The other interesting observation is that, compared with the absorption and SAXS data, the WAXRD data in the demineralized region seem to return to the sound level in the shallower region: WAXRD recovers at around 80 μm, while the changes in the absorption and the SAXS persist more than 100 μm. This is discussed in details below.

4. Discussion

Demineralization of tooth enamel is loss of minerals from the enamel subsurface lesion (Silverstone, 1977). The phenomenon of demineralization is usually determined by TMR, which measures the amount of minerals by X-ray microradiography. However, since TMR measures X-ray absorption by an enamel slice, the amount of HAp crystallites cannot be determined. The present report is the first one on the direct detection of changes in the amount of the HAp crystallites in the enamel subsurface lesion by microbeam X-ray diffraction. We used three different X-ray techniques on the same sample to investigate the structure of the subsurface lesion at different structural levels. TMR (and transmission measurement)
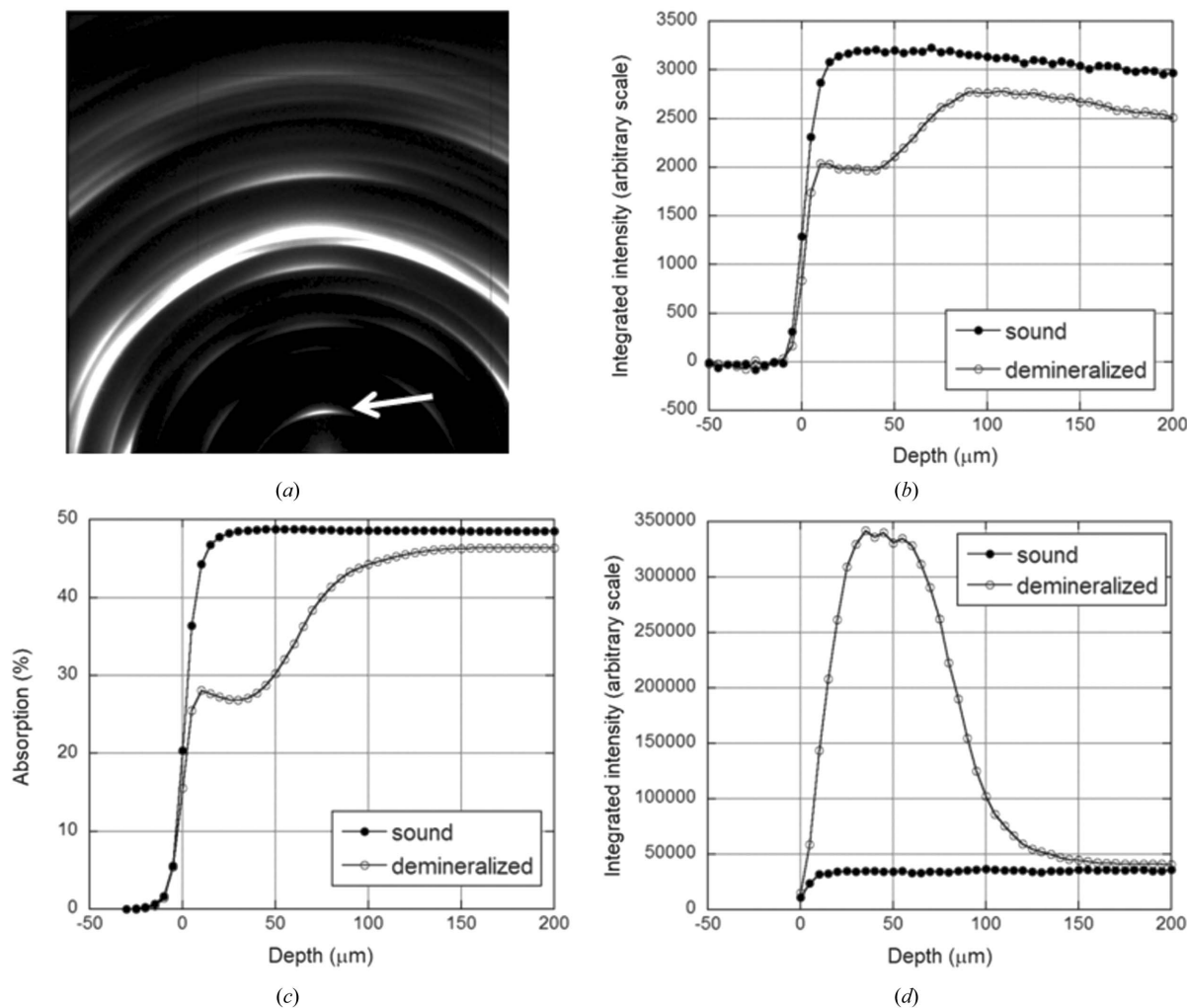
Figure 5
Data on bovine enamel by the simultaneous SAXS/WAXRD/transmission measurement. (*a*) WAXRD pattern recorded by a CMOS flat-panel detector from the sound zone. The arrow indicates the equatorial (100) reflection. The exposure time was 1.0 s. The background recorded without the sample was subtracted with a correction for absorption. (*b*) Change in the integrated intensity of the equatorial (100) reflection from the surface to the deeper region of the sound and demineralized zones. (*c*) Change in the absorption of X-rays by the enamel slice in the sound and demineralized zones. (*d*) Change in the integrated intensity of the small-angle scattering from the surface to the deeper region of the sound and demineralized zones. The plots are an average of data from three samples of different teeth. Normalization was not applied.

showed the amount of minerals in the subsurface lesion, WAXRD showed the amount of HAp crystallites, and SAXS showed the formation of voids caused by the loss of HAp from crystallites.

The results of these three measurements showed strong correlations in the depth profiles. The demineralization of enamel (Fig. 2) is concurrent with the decrease of the HAp crystallites (Fig. 3*b*) and the increase of the voids (Fig. 4*b*) which has been found with electron microscopy (Featherstone, 1979; Kerebel *et al.*, 1979). These results illustrate loss of crystalline HAp at different structural levels, demonstrating that the demineralization in the subsurface lesion accompanies loss of the HAp crystallites.

Although X-ray diffraction has been used to characterize HAp in tooth enamel over 50 years, the spatial resolution required to examine the subsurface lesion has become available only recently. Since the three X-ray techniques TMR, WAXRD and SAXS report on different aspects of lesion, the results are not always quantitatively the same. For instance, TMR measures absorption which changes exponentially with the mass in the X-ray beam, while WAXRD originates from the HAp crystallites and its intensity depends not only on their volume but on other factors such as crystal sizes and regularity of the crystals. The origin of the SAXS is the voids formed in the enamel as a result of decrease in the crystallite volume and its intensity depends more on the surface area than the void volume (Porod's law) (Ciccariello *et al.*, 1988). Thus, the three methods provide complementary information on the enamel structure. For instance, TMR cannot discriminate HAp crystallites from other precipitate such as calcium phosphate, while the lack of diffraction spots other than those from HAp indicates that there is not a significant amount of crystals other than HAp. Thus, it will be useful to compare results of the three measurements under different conditions to study the mechanism of demineralization of tooth enamel.

In the data in Fig. 5, the WAXS result (Fig. 5b) seems different from the absorption (Fig. 5c) and SAXS (Fig. 5d) results in that the intensity in the demineralized enamel recovers to the sound level at a depth less than 100 μm, while the absorption and the SAXS intensity do not recover fully up to 150 μm. This suggests that, although the amount of the crystalline HAp is unchanged, there are some structural changes in the 100–150 μm region. These may be happening in the matrix between HAp crystals: for example, the density of the matrix may be lowered, or there may be small cracks. These possibilities may be further investigated by electron microscopy.

The demineralization in the early caries lesion may be reversed by calcium and phosphate in saliva (Silverstone, 1977; Featherstone, 2004; Dowd, 1999; ten Cate *et al.*, 1981). Many studies are carried out to facilitate this remineralization process using chemical substances (Winston & Bhaskar, 1998). Thus, the techniques presented in this paper may be instrumental in studying the structural basis of remineralization. We have already obtained interesting results on remineralization, which will be published elsewhere (Tanaka *et al.*, 2009).

References

Amemiya, Y., Ito, K., Yagi, N., Asano, Y., Wakabayashi, K., Ueki, T. & Endo, T. (1995). *Rev. Sci. Instrum.* **66**, 2290–2294.

Arends, J. & Christoffersen, J. (1986). *J. Dent. Res.* **65**, 2–11.

Arends, J. & Jongebloed, W. L. (1978). *J. Biol. Buccale*, **6**, 161–171.

Ciccariello, S., Goodisman, J. & Brumberger, H. (1988). *J. Appl. Cryst.* **21**, 117–128.

Crawshaw, J. & Cameron, R. (2000). *Polymer*, **41**, 4691–4698.

Damen, J., Exterkate, R. & ten Cate, J. (1977). *Adv. Dent. Res.* **11**, 415–419.

Dowd, F. J. (1999). *Dent. Clin. N. Am.* **43**, 579–597.

Featherstone, J. & Zero, D. (1992). *J. Dent. Res.* **71**, 804–810.

Featherstone, J. D. (1979). *J. Ultrastruct. Res.* **67**, 117–123.

Featherstone, J. D. B. (2004). *J. Dent. Res.* **83**(Spec. Iss. C), C39–C42.

Fraser, R. & MacRae, T. (1974). *Conformation in Fibrous Proteins and Related Synthetic Polypeptides.* New York: Academic Press.

Gupta, A., Harrison, I. R. & Lahijani, J. (1994). *J. Appl. Cryst.* **27**, 627–636.

Gutierrez, P., Piña, C., Lara, V. & Bosch, P. (2005). *Arch. Oral Biol.* **50**, 843–848.

Hirota, F. (1986). *J. Dent. Res.* **65**, 978–981.

Inoue, K., Oka, T., Suzuki, T., Yagi, N., Takeshita, K., Goto, S. & Ishikawa, T. (2001). *Nucl. Instrum. Methods*, A**467–468**, 674–677.

Kerebel, B., Daculsi, G. & Kerebel, L. M. (1979). *J. Dent. Res.* **58**(Spec. Iss. B), 844–851.

Meyer-Lueckel, H., Tschoppe, P. & Kielbassa, A. (2006). *J. Oral Rehab.* **33**, 760–766.

Ohta, N., Oka, T., Inoue, K., Yagi, N., Kato, S. & Hatta, I. (2005). *J. Appl. Cryst.* **38**, 274–279.

Silverstone, L. (1977). *Caries Res.* **11**(Suppl. 1), 59–84.

Simmelink, J. & Abrigo, S. (1989). *Adv. Dent. Res.* **3**, 241–248.

Tanaka, T. *et al.* (2009). In preparation.

ten Cate, J., Dundon, K., Vernon, P., Damato, F., Huntington, E., Exterkate, R., Wefel, J. S., Jordan, T., Stephen, K. W. & Roberts, A. J. (1996). *Caries Res.* **30**, 400–407.

ten Cate, J., Jongebloed, W. L. & Arends, J. (1981). *Caries Res.* **15**, 60–69.

Trautz, O., Klein, E., Fessenden, E. & Addelston, H. (1953). *J. Dent. Res.* **32**, 420–431.

Winston, A. E. & Bhaskar, S. N. (1998). *J. Am. Dent. Assoc.* **129**, 1579–1587.

Yagi, N. & Inoue, K. (2007). *J. Appl. Cryst.* **40**, s439–s441.